PCCP

ROYAL SOCIETY OF CHEMISTRY

PAPER

Published on 21 September 2026
Licensed under CC-BY 4.0

Check for updates

Cite this: DOI: 10.1039/d6cp01691j

Assessing sequence reversal effects on coiled-coil stability using AI-based structure prediction and enhanced sampling atomistic simulations

Maria Arnittali,[a] Elena Markopoulou,[b] Vagelis Harmandaris [cde] and Anastassia N. Rissanou *[f]

This study investigates the impact of sequence inversion on the structural integrity and thermodynamic stability of the wtRop protein, a prototypical coiled-coil motif. We utilized AI-driven structure prediction (ColabFold) to generate initial models for the unknown rRop sequence, which yielded both parallel and antiparallel monomeric orientations. These models were subjected to classical molecular dynamics simulations and well-tempered metadynamics. The combination of atomistic simulations and enhanced sampling techniques allowed for the calculation of the free energy surface across four collective variables: (i) angle between the monomers, (ii) distance between the monomer's center of mass, (iii) helicity and (iv) torsion angle similarity, characterizing the energetic barriers and conformational transitions of the parallel rRop, the antiparallel rRop, and the parent wtRop systems. Free energy analysis reveals that both rRop models deviate from the native antiparallel orientation to stabilize at an intermediate angle. Notably, the antiparallel variant exhibits the most significant instability, characterized by increased monomer separation and a more pronounced loss of secondary structure relative to the wild-type and the parallel model. While both reversed sequences show a reduction in α-helicity compared to wtRop, the antiparallel model demonstrates a more pronounced loss of structural integrity, characterized by a disrupted hydrogen bond network, increased solvent-accessible surface area, and the failure to maintain a robust hydrophobic core. Free energy calculations further confirmed that the parallel variant shares greater conformational similarity with the parent protein.

Received 7th May 2026,
Accepted 18th September 2026

DOI: 10.1039/d6cp01691j

rsc.li/pccp

1. Introduction

Proteins are fundamental to almost all biological processes, and their structure plays a critical role in determining their function. It is well known that even small changes in protein sequence disrupt the molecule's physiological conformation and are often found to be the leading cause of pathogenesis of various neurodegenerative disorders like Alzheimer's[1] and Parkinson's.[2] Therefore, an emerging methodology in materials design is strategically modifying well known protein sequences or motifs to alter their functionality. Understanding the relationship between protein sequence, structure, and dynamics is essential for advancing fields such as drug design, enzyme engineering, and synthetic biology.[3–6] Among the various protein motifs, coiled-coil structures are of particular interest due to their simplicity, stability, and the ability to design them with desired properties.[7–10]

A well-known example of a coiled-coil structure is that of Rop (repressor of primer) protein which constitutes an excellent model system for studying protein folding, stability, and conformational dynamics.[7] The native wild-type Rop (wtRop) protein consists of two identical polypeptide chains that form an antiparallel dimeric coiled-coil structure. Each polypeptide chain consists of two antiparallel α-helices connected by a short loop of 5 residues resulting in an α-helical hairpin configuration.[7,8] The dimeric coiled-coil structure is stabilized by a combination of hydrogen bonding and hydrophobic interactions, which maintain the protein's structural integrity under various environmental conditions.[9] The Rop protein is involved in the regulation of plasmid copy number in *Escherichia coli*, a

[a] Department of Computer Science School of Sciences and Engineering, University of Nicosia, 46 Makedonitissas Avenue, 2417, Nicosia, Cyprus
[b] Department of Materials Science and Engineering, University of Crete, GR-71409 Heraklion, Crete, Greece
[c] Department of Mathematics and Applied Mathematics, University of Crete, GR-71409, Heraklion, Crete, Greece
[d] Institute of Applied and Computational Mathematics, Foundation for Research and Technology Hellas, IACM/FORTH, GR-71110 Heraklion, Crete, Greece
[e] Computation-Based Science and Technology Research Center, The Cyprus Institute, Nicosia, Cyprus
[f] Institute of Theoretical and Physical Chemistry, National Hellenic Research Foundation, 48 Vassileos Konstantinou Ave, Athens 11635, Greece. E-mail: trissanou@eie.gr

function that depends on its ability to adopt a stable dimeric conformation.[10] The stability and well-characterized nature of wtRop have made it a subject of extensive research,[9,11–13] allowing scientists to probe the fundamental principles governing coiled-coil formation and stability. In a recent study of our group, we explored the role of wtRop protein's loop region in the physical properties and the secondary structure of the protein, such as its conformational and thermal stability.[9] More specifically, by combining Molecular Dynamics simulations and circular dichroism spectroscopy, this study concluded that the loop region is one of the most flexible regions of the structure while the residues constituting the protein's α-helices are more thermostable.

Recent advances in protein engineering have opened new possibilities for manipulating protein structures to explore the effects of sequence modifications.[11,13–15] One such modification involves sequence reversal, where the amino acid sequence is reversed while attempting to preserve the original heptad repeat pattern which is typical of coiled-coil motifs. This process can yield reversed-sequence variants of proteins which retain the general sequence characteristics of the original protein but with the amino acids arranged in the opposite order.[16,17] These engineered variants provide a unique opportunity to investigate how sequence directionality influences protein folding, stability, and function.[11,16,18,19] However, the structural and dynamic properties of reversed-sequence proteins are not as straightforward as their native counterparts. The reversal of the primary sequence can potentially cause dramatic changes in the overall folding and stability of the protein, since the positions of critical residues responsible for hydrophobic interactions and hydrogen bonding are altered.[18,20,21] Foundational studies on coiled-coil and helical-bundle systems provide useful context for interpreting sequence-reversal effects. Using lattice Monte Carlo simulations, Olszewski, Kolinski and Skolnick investigated whether the reversed sequence of a three-helix-bundle protein (retro-protein A, derived from the B domain of Staphylococcal protein A) folds into a well-defined, native-like structure.[22] They found that the retro-sequence retained the ability to fold into a compact helical bundle, but its topology and helix packing differed from those of the parent protein, indicating that sequence reversal preserves foldability without necessarily conserving the native fold. In a complementary experimental study, Mittl *et al.* determined the crystal structure of the retro-GCN4 leucine zipper and found that, in contrast to the native two-stranded parallel coiled-coil dimer, the reversed sequence instead assembled into a markedly different, highly stable parallel four-helix bundle.[23] These early studies established that sequence reversal, while generally compatible with folding into ordered helical structures, can substantially alter the oligomeric state and packing arrangement relative to the parent protein. More recent computational studies have extended these findings using modern simulation approaches. Zerze *et al.*[24] employed all-atom, enhanced-sampling molecular dynamics simulations to characterize the equilibrium structures of retro-isomer peptides, underscoring the value of advanced sampling methods, such as the well-tempered metadynamics approach, for accurately capturing the conformational landscape of reversed-sequence proteins. Across various studies, even subtle sequence or structural changes have been reported to cause major shifts in stability and folding pathways,[4,25–27] making the study of reversed-sequence proteins an intriguing area of research.

Like its wild-type counterpart, reverse wtRop (rRop) serves as an excellent model system for investigation. Over the years, numerous mutations have been applied on the structure of the Rop protein, such as single amino acid replacement or removal of the loop region,[15,25,26,28,29] in an attempt to decipher the folding mechanism of coiled coil proteins. However, the specific effects of sequence reversal on the stability and structural dynamics of the Rop protein remain largely unexplored. An experimental analysis of the folding of rRop and comparison to its parent protein by Kefala *et al.* identified the adoption of a highly flexible, native-like structure of looser packing by rRop through a complex mechanism.[19] Furthermore, a more recent study of our group combining computational and experimental techniques also indicates that sequence reversal disrupts the hydrophobic core of Rop, leading to the formation of additional secondary structures.[17] Computational findings of this study suggest a dimeric conformation of rRop as the more likely to a monomeric one, but further exploration of rRop's free energy landscape is necessary to increase prediction accuracy.

Despite the inherent difficulties in resolving 3D protein structures, the field is being transformed by computational advances in machine learning methods. To this day, AlphaFold is one of the most efficient tools of this kind, with the ability to reach near-experimental accuracy.[30,31] This is accomplished by combining training methods, based on scattering (PDB) data, which represent the whole range of conditions that known structures have been solved, with innovative neural network topologies.[31–34] In the current study, AlphaFold was used to predict the structure of rRop protein producing two possible configurations, one with parallel arrangement of Rop's monomers and one with antiparallel arrangement of the monomers. In the following we refer to the monomers as Ma and Mb. However, limitations in the availability of training data for reversed-sequence proteins make further verification of the predicted structures necessary.[33,35,36]

Here, in order to validate the two reverse models, we investigate the structural stability and dynamics of the two suggested configurations of rRop and compare them to the native wtRop. We employed two computational approaches, classical molecular dynamics (MD) simulations and enhanced sampling techniques, to explore the conformational landscapes of these proteins. Traditional MD simulations are effective for capturing the time-dependent behavior of proteins but are often limited by the energy barriers that prevent exploration of less favorable conformations. To overcome these limitations, we utilized Well-Tempered Metadynamics (WTmetaD), an advanced sampling method that allows the system to escape local energy minima and explore a wider range of conformational states.[37–40]

More specifically, the more thorough exploration of a system's free-energy landscape *via* WTmetaD detects all the accessible conformations under experimentally relevant conditions, enabling us to single out the most probable ones.[37,41] Furthermore, these calculations give vital details regarding the magnitude of the energy barriers between the dominant minima which highlight

 This journal is © the Owner Societies 2026

the pathway of conformational transitions by identifying metastable states.[42] Metadynamics simulations have been previously employed to explore the metastable landscapes of various protein systems. In a recent study, Nadwa *et al.*,[43] investigated the early misfolding steps of serum amyloid A (SAA) by employing parallel-tempering metadynamics (PT-MetaD) and harmonic linear discriminant analysis (HLDA) for enhanced sampling of the SAA1-76 fragment. It was found that Helix III destabilizes first, leading to subsequent unfolding of helices II and I, whereas the overall compactness remains stable despite the loss of secondary structure. Another interesting work utilizes variationally augmented contact metadynamics[44] to investigate protein conformational transitions using path collective variables (PCVs) on L99A T4 Lysozyme. Beyond identifying the slow transition modes between the metastable G and E states, the simulation revealed two distinct intermediate states. The resulting free energy calculations demonstrated strong agreement with experimental benchmarks. Gong *et al.* employed WTmetaD, among other simulation techniques, to uncover the mechanisms that govern ligand-induced conformational transitions of the LRRK2 enzyme providing vital information for Parkinson's disease therapeutics.[45]

Overall, the systematic exploration of conformational regions of interest and the bias-eliminating properties of WTmetaD are particularly beneficial for enhancing our understanding of the mechanisms that trigger protein bioactivity, in other words the processes that shift a protein's conformation in a way that exposes the active site to its surroundings,[38,39,41,46] or for ligands to attach to protein surfaces.[46–50]

In this study, examining energy landscapes allowed us to evaluate the stability of wtRop and rRop proteins, while characterizing the ease of transition between their conformational states. We investigated two rRop models based on AlphaFold predictions, one with parallel monomer orientation and the other with antiparallel orientation. Our findings contribute to a deeper understanding of how sequence reversal affects the folding and stability of coiled-coil proteins and offer insights into the design principles that can be applied to synthetic protein engineering. Overall, this study aims to bridge the gap in understanding the impact of sequence directionality on protein conformational preferences by providing a detailed comparison between the native wtRop and its reversed-sequence variants. By combining classical MD simulations, artificial intelligence (AI) tools and enhanced sampling techniques, we target on elucidating the structural and dynamic profiles of these proteins and establish a framework for future developments in synthetic protein design. Our results have broader implications for the development of novel biomolecules with tailored stability and functionality, which are critical for various biotechnological and therapeutic applications.

2. Materials and methods

2.1. Protein models

The native structure of the wtRop protein is well-characterized, and its original structural data sourced from the Protein Data Bank (PDB code: 1RPR).[8] Hydrogen atoms and protonation state were assigned during topology generation in GROMACS. The experimental structure was inspected for structural completeness, and no missing residues requiring additional modeling were identified. Due to the lack of experimental structures for rRop, in a previous study of our group[17] we used the PyMol software package[51] to build a dimeric antiparallel model, utilizing wtRop as a structural scaffold. The conformational properties of the model were characterized through molecular dynamics simulations. In the present study, we used the AlphaFold AI system to predict the 3D structure of rRop, based solely on its amino acid sequence. Due to the substantial computational resources required by AlphaFold,[31] ColabFold was employed, which runs on a web-based platform and eliminates the need for local processing or large-scale data storage. ColabFold generated five structural models of rRop: four exhibited a parallel orientation between monomers (Fig. 1A), while one adopted an antiparallel orientation (Fig. 1B), consistent with our previous constructed model for rRop.

2.2. Classical MD simulation

All-atom molecular dynamics (MD) simulations were performed using the GROMACS software package[52] (GROMACS 5.0.7). Inter- and intramolecular interactions for all protein models were described using the GROMOS 53a6 force field,[53] and water was described using the SPC/E explicit solvent model.[54] Each protein was placed in a cubic simulation box with dimensions of $9 \times 9 \times 9$ nm^3 and periodic boundary conditions were applied in all three directions. Na^+ ions were added to neutralize the systems. Prior to production simulations, each system was subjected to energy minimization using the steepest-descent algorithm, with a maximum of 50 000 minimization steps and an initial step size of 0.01 nm. Energy minimization was considered converged when the maximum force was below 1000 kJ mol^{-1} nm^{-1}. Production simulations were performed using leap-frog integrator. Temperature was controlled using the stochastic velocity rescaling thermostat[55] maintaining the system at 300 K with a coupling constant of 0.1 ps. Pressure coupling

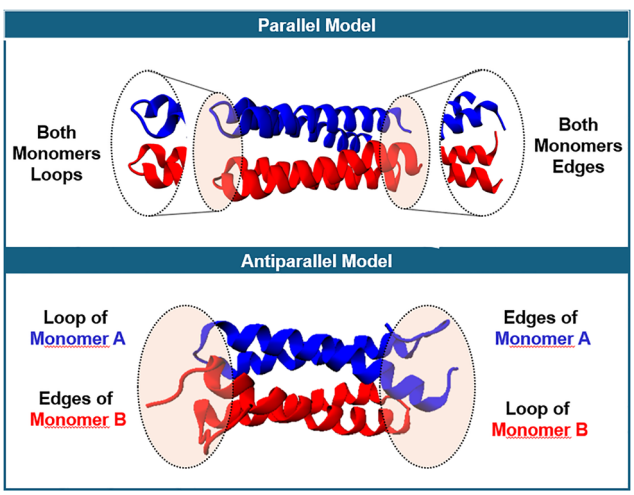


Fig. 1 Graphical representation of the two different conformations of rRop generated by ColabFold: (top panel) parallel orientation and (bottom panel) antiparallel orientation of the monomers.

Table 1 Simulation details of all systems including the total number of atoms ("Atoms"), the number of water molecules ("Water mol."), the number of added ions to neutralize the systems ("Ions"), and the simulation time (t)

Systems	Atoms	Water Mol.	Ions	t (μs)
rRop (parallel)	71 299	23 335	14	0.5
rRop (antiparallel)	72 037	23 575	14	2
wtRop	73 861	24 189	14	0.275

was performed using the Berendsen barostat[56] to keep the system close to the target pressure (1 atm) and to ensure numerical stability in combination with the metadynamics bias potential. Since the properties investigated in this study do not rely on the accurate sampling of pressure/volume fluctuations, the well-known limitations of this barostat, in this respect do not affect the reported results. Electrostatic interactions were calculated using the particle mesh Ewald (PME) method with a cutoff distance of 1.0 nm. A time step of 1 fs was used to integrate the equations of motion. Simulation details for all systems are summarized in Table 1, including the total number of atoms, the number of water molecules, the number of Na^+ ions added for system neutralization, and the simulation time (t). Each system comprised a single homodimer protein. To assess reproducibility, one additional independent long MD simulation was performed for each of the two rRop models (parallel and antiparallel). The resulting structural properties were consistent between replicas, with the differences falling within the associated error bars (Fig. S9, S12 and Tables S1, S2).

This study primarily investigates the parallel configuration of rRop, which is the top-ranked prediction by AlphaFold, and evaluates its features through comparisons with the antiparallel rRop and wtRop models.

2.3. Well-tempered metadynamics simulations

Well-tempered metadynamics (WTmetaD) simulations were performed to map the conformational space for all three models (wtRop, rRop parallel, and rRop antiparallel). These simulations were performed using GROMACS version 2016.4 and PLUMED version 2.4.1 plugin. Initial configurations for the WTmetaD simulations were derived from unbiased Molecular Dynamics trajectories, as illustrated in Fig. 2. To ensure the simulations originated from thermodynamically stable, low-energy states, the structural equilibrium of these starting points was verified through rmsd analysis (Fig. 4A and Fig. S11). This is particularly relevant for the rRop models, since wtRop, being in its native state, is assumed to be at the global minimum. The system setup for the WTmetaD simulations was identical to that described in Table 1.

The duration of the WTmetaD simulations ranged from 0.1 to 0.5 μs, utilizing MD parameters consistent with those described in Section 2.2. We identified suitable collective variables (CVs), which are essential for ensuring both the efficiency and accuracy of the WTmetaD technique.[57] In the present study, four collective variables (CVs) were employed, with Gaussian widths (σ) derived from the standard deviations observed in unbiased MD simulations. These σ values were specifically determined using block-averaging analysis for each protein model. Gaussian heights of 0.9, 1.0, and 1.2 kJ mol^{-1} were utilized, along with two bias factors of 10 and 15. The bias factor was tuned empirically for each rRop model to ensure adequate crossing of the relevant free-energy barriers within the simulated timescale.[58] Four independent WTmetaD simulations were performed for each protein model, one for each of the four collective variables (θ, r_{cm}, H, and S). A detailed description of the selected CVs is provided in the SI. Convergence of the WTmetaD simulations was assessed using two complementary indicators. First, the time evolution of the deposited Gaussian hill heights was monitored; within the well-tempered scheme, the bias deposition rate progressively decreased, and the Gaussian heights approached negligible values, indicating that the bias potential was no longer substantially modifying the estimated free-energy landscape. Second, free energy surfaces (FESs), reconstructed at successive simulation time windows were compared: the locations and relative depths of the main free-energy minima remained essentially unchanged during the final part of the simulation, indicating that the FES has reached a quasi-stationary state. Fig. S13A, B and S13C, D show this evidence for both CV1 (θ) and CV2 (r_{cm})

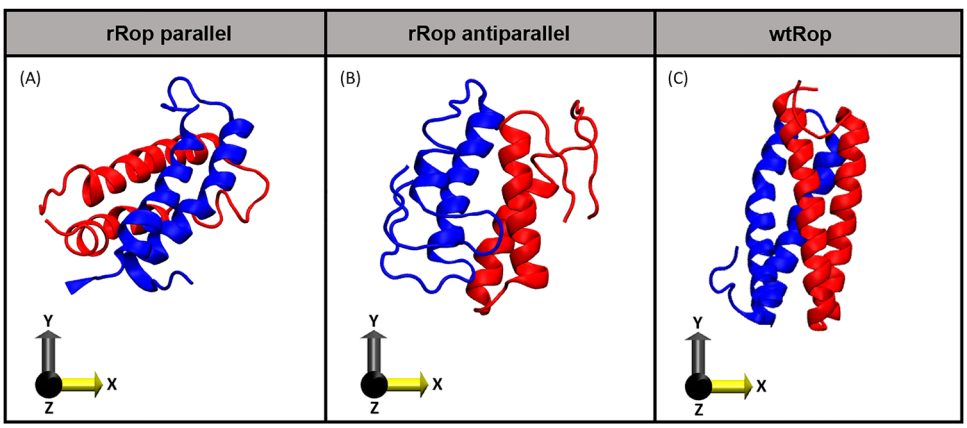


Fig. 2 Snapshots of the starting structures of (A) rRop parallel, (B) rRop antiparallel and (C) wtRop protein models for WTmetaD simulations. Monomer A is shown in red, and monomer B in blue. All three structures are superposed on a common reference frame, obtained by aligning monomer A of each model onto monomer A of wtRop (Cα backbone rigid-body fit). For clarity, the water molecules are omitted.

This journal is © the Owner Societies 2026

respectively. Additionally, the time evolution of the selected CVs from the classical MD simulations were shown in Fig. S2–S5. The corresponding time evolution of the CVs during the biased WTmetaD simulations is presented, indicatively for the parallel rRop model, in Fig. S6 (inter-monomer CVs, θ and r_{cm}) and Fig. S7 (intra-monomer CVs, H and S) in the SI.

3. Classical MD simulations of parallel rRop

3.1. Conformational analysis

We conducted 0.5 μs simulations of the parallel rRop model at 300 K and 1 atm. A visual comparison of the initial and final configurations is provided in Fig. 3A and B, respectively. Notably, the final configuration reveals a structural rearrangement of the two monomers. This loss of orientation suggests that the parallel dimeric conformation is inherently unstable. Corresponding observations of both wtRop and rRop antiparallel,[9,17] reveal preserved structural integrity for wtRop, in contrast to the antiparallel rRop, where significant structural perturbation occurs. Initial and final configurations are presented in Fig. S8A and B for antiparallel rRop and Fig. S8C and D for wtRop respectively.

Calculations of the root mean square deviation (rmsd) and the root mean square fluctuation (rmsf) provide quantitative measures for the structural stability and the most flexible parts of the protein. In the literature, rmsd values between 0.15 nm and 0.25 nm typically indicate high structural similarity to the reference structure.[59] For the parallel rRop model, this reference corresponds to the initial conformation predicted by AlphaFold. The rmsd and rmsf analyses were performed using the Cα carbon atoms of all amino acids in each protein. The mean rmsd values and their associated uncertainties were determined using the block averaging method. Unless otherwise stated, all structural and thermodynamic properties were computed over the equilibrated part of each trajectory, based on the time evolution of rmsd (*i.e.*, beyond 100 ns for rRop parallel model (Fig. 4A, blue line); beyond 200 ns for rRop antiparallel (Fig. 4A, orange line); beyond 150 ns for wtRop (Fig. 4A, green line)).

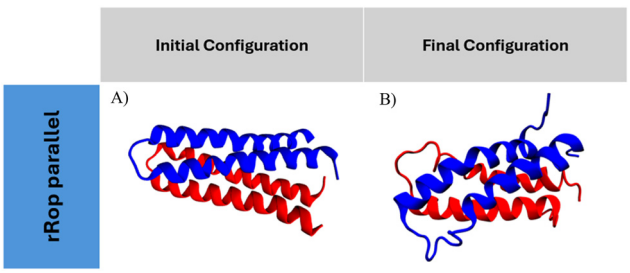


Fig. 3 Characteristic snapshots of (A) initial configuration (t = 0) and (B) final configuration (t = 0.5 μs) of the parallel rRop model. For reasons of clarity, the water molecules and ions are omitted.

The rmsd as a function of time for the rRop models, together with the wtRop parent protein, is presented in Fig. 4A. Reported rmsd values for the rRop models represent the average of two independent simulation runs. Following an initial rise, the rmsd of the parallel model stabilizes after 100 ns at ∼0.44 nm. The antiparallel model stabilizes at an even higher value, ∼0.8 nm, while wtRop stabilizes at a markedly lower value, ∼0.3 nm, confirming its native structural stability. This trend indicates that both reversed-sequence models are structurally less stable than the native protein, with the antiparallel model showing the most pronounced deviation. Fig. S11 in the SI illustrates the rmsd time evolution of the antiparallel rRop over 2 μs trajectory, confirming that the ∼0.8 nm plateau remains stable over this extended timescale. Although both rRop models deviate significantly from their reference structures, the parallel configuration exhibits greater comparative stability than the antiparallel one.

The rmsf as a function of residue index for all three protein models is presented in Fig. 4B. For rmsf calculations, the values per residue are presented as the mean values per residue averaged over both monomers. Values were calculated over the stabilized part of the trajectory for each system. Both rRop models exhibit consistently higher rmsf values than wtRop, reflecting greater conformational instability across all regions. In all models, the

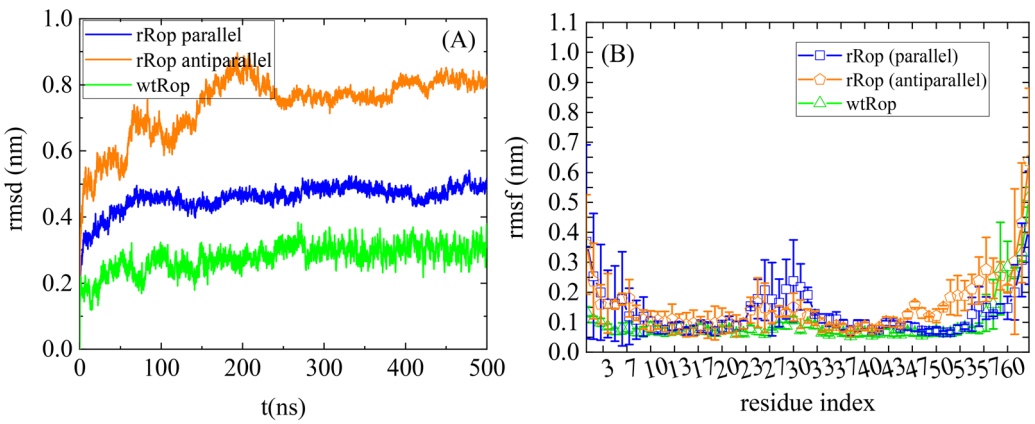


Fig. 4 (A) Time evolution of the root mean square deviation (rmsd) of the Cα atoms of wtRop and rRop parallel and antiparallel protein models. rmsd values for rRop are given as the average across two independent simulation runs; (B) the root mean square fluctuation (rmsf) of the Cα atoms per residue for the three models.

C-terminal region [residues 58–63] exhibits the highest rmsf values, reflecting the characteristic high mobility of these terminal residues. Moreover, the rRop antiparallel model displays elevated fluctuations in α-helical regions [residues 13–20] and [residues 45–57], suggesting reduced helical stability compared to the parallel model. On the contrary, the rRop parallel model exhibits pronounced instability in the loop region [residues 28–32].

To further dissect the origin of the structural deviations captured by the total rmsd, we additionally computed the rmsd of each monomer individually relative to its own initial configuration (intra-monomer rmsd), thereby isolating monomer-intrinsic structural changes from the global rmsd, which couples both intra- and inter-monomer contributions. For the rRop parallel model, both monomers display closely comparable intra-monomer rmsd throughout the trajectory (Fig. S10B), indicating a similar degree of internal structural change. In contrast, the rRop antiparallel model shows a pronounced asymmetry between monomers, with monomer B consistently exhibiting larger and more variable intra-monomer rmsd than monomer A (Fig. S10A), pointing to a more substantial, monomer-specific structural rearrangement; wtRop displays only a modest asymmetry between monomers (Fig. S10C). This monomer-resolved picture is consistent with the greater overall instability of the antiparallel model already indicated by the total rmsd and rmsf metrics (Fig. 4), and is further supported by the hydrogen bonding, SASA, and hydrophobic core analyses presented below.

In the following, we perform secondary structure analysis on the parallel rRop model, which exhibits comparatively greater structural stability among the two reversed-sequence models and provides a more detailed, residue-level quantification of how the amino acid sequence determines the structure attained by the protein. The secondary structure of the antiparallel rRop and wtRop models has been characterized in our previous publications.[9,17] The secondary structure of the parallel model as a function of time is presented in Fig. 5, where the y axis represents the residue id. The analysis was performed using the DSSP algorithm,[60] classifying the structures as coil (grey), β-sheet (red), β-bridge (black), bend (green), turn (yellow), α-helix (blue), π-helix (purple), and 310-helix (magenta). Significant changes in the secondary structure of the parallel rRop model occurred over the 500 ns simulation. Specifically, the α-helical content decreased by 28.6% relative to the initial configuration. Despite this reduction, α-helices (blue) remain the dominant structural motif. Of particular interest is the presence of π-helix (purple) in monomer B after ∼10 ns. In striking contrast, the antiparallel rRop model exhibited significant structural perturbation and the DSSP analysis revealed a 53.06% reduction in α-helical content when comparing the final configuration to the initial state (Fig. S8A and B).

The time evolution of the number of residues adopting α-helical conformation in the rRop parallel model is presented in Fig. 6. A sharp decline in α-helical content occurs within the first 100 ns, of the trajectory, which indicates fast conformational dynamics, followed by a gradual evolution that stabilizes at approximately ∼68 residues after ∼400 ns.

3.2 Hydrogen bonds

Hydrogen bonds (HBs) are essential to the formation and stabilization of protein structures. To assess how HB disruption contributes to rRop instability, we quantified several classes of interactions: inter-monomer HBs (Ma–Mb), intra-monomer HBs (Ma–Ma and Mb–Mb), and total protein–protein HBs (P–P), which is the sum of all intra- and inter- monomer HBs. Additionally, protein–solvent interactions were evaluated *via* protein–water HB analysis. HBs were identified using standard geometric criteria: distance: (D···A) ≤ 0.35 (nm) and angle (D–H···A) ≤ 30°, between donor (D) and acceptor (A) atoms. Table 2 presents the average number of hydrogen bonds (including both backbone and side chains) for all models, with values and associated uncertainties computed *via* block averaging over the stabilized part of each trajectory. For the rRop parallel and antiparallel models, the values reported in Table 2 represent the averages obtained across the two independent MD simulations runs. The corresponding results for each individual replica are provided in Table S1 of the SI.

Both rRop models exhibited significant reductions in the total number of HBs (P–P) compared to the wtRop model. Specifically, the average number of P–P HBs decreased by approximately 15.8% and 17.3% for parallel and antiparallel rRop models, respectively. Differences were also observed in

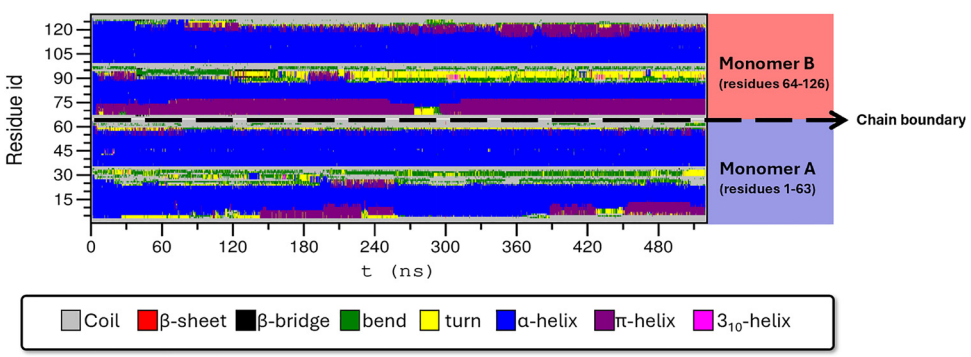


Fig. 5 Analysis of the Secondary Structure of Protein (DSSP) of rRop parallel throughout the simulation time. The secondary structure content was evaluated with the DSSP algorithm: coil (gray), β-sheet (red), β-bridge (black), bend (green), turn (yellow), α-helix (blue), π-helix (purple), and 3_{10}-helix (magenta). Residue id <64 represents monomer A and residue id ≥64 represents monomer B. Black dashed line separates the two monomers.

 This journal is © the Owner Societies 2026

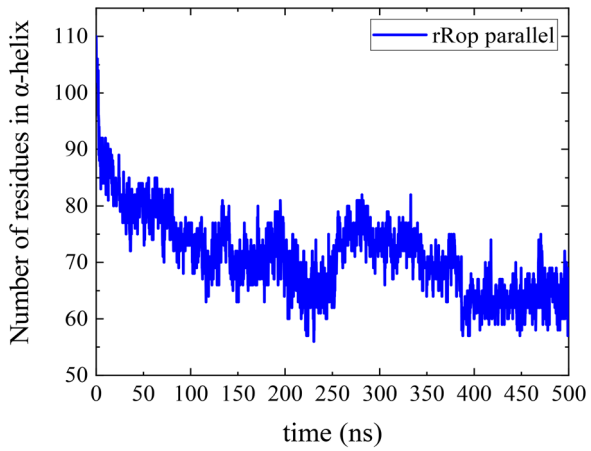


Fig. 6 Number of residues involved in the formation of α-helix with respect to the simulation time of the rRop parallel model.

the inter-monomer HBs (Ma–Mb). The parallel rRop model exhibited a modest decrease of approximately 9.2% relative to wtRop, whereas the antiparallel model showed an increase of approximately 23.6%, suggesting either a partial removal of the monomers or significant orientational shifts. More pronounced reductions were observed in the intra-monomer HBs (Ma–Ma and Mb–Mb), which decreased by approximately 15–23% in both rRop models. This decline suggests a substantial disruption of the secondary structure within the individual protein subunits. Consistent with the loss of P–P HBs, both rRop models exhibited a rise in protein–water (P–W) HBs. Both the parallel and antiparallel variants showed approximately 8.4% more P–W HBs than the wild-type protein, pointing to an increased hydration of the monomers. This enhanced solvent exposure will be further examined through subsequent solvent accessible surface area (SASA) analysis.

3.3. Solvent accessible surface area (SASA) and hydrophobic contacts

Taking into account the increase of the HBs between water molecules and the rRop proteins, we computed the solvent accessible surface area (SASA) and the hydrophobic contacts (HCs) for the three protein models. SASA is a measure of the surface area of a molecule that is reachable by solvent molecules. Table 3 includes the average SASA values for all the proteins studied. The reported values for both rRop models are given as the average across the two independent simulation runs. The corresponding results for each individual replica are provided in Table S2 of the SI. Both rRop models exhibited significantly higher SASA values compared to those of the wtRop protein, indicating a larger surface area accessible to water molecules in the reversed models, which aligns with our findings for the increase in the number of HBs between water molecules and protein.

Table 3 Average values of SASA of the three protein models. SASA values for rRop models are given as the average across two independent simulation runs

Systems	SASA (nm^2)
rRop parallel	78.99 ± 0.73
rRop antiparallel	80.70 ± 0.28
wtRop	73.9 ± 0.24

By monitoring the SASA over time, presented in Fig. 7, a further evaluation of the conformational dynamics is provided. While the SASA of the wtRop protein remained stable throughout the simulation, the rRop models exhibited significant temporal variations, indicating transitions between conformational states. They initially underwent increased solvent exposure before their SASA values decreased, suggesting structural rearrangements relative to their starting structures. This trend is particularly pronounced in the antiparallel model. In contrast, the parallel rRop showed a SASA reduction up to ∼200 ns, reflecting similar conformational dynamics observed in the α-helix time dependence (Fig. 6).

The coiled coil motif has a characteristic feature which is the presence of the heptad repeat pattern, where hydrophobic, hydrophilic and charged residues occupy specific positions in a periodic arrangement. Following the classification scheme of Kefala *et al.*,[19] the residues of wtRop and rRop proteins were classified into hydrophobic, hydrophilic and charged groups. Subsequently, we investigated the hydrophobic contacts (HC) and their role in forming a hydrophobic core across all examined systems. In the wtRop protein, hydrophobic residues occupy positions "a" and "d" within the heptad repeat pattern. Upon reversing the sequence, the residues originally located at position "d" are now situated at position "a", and *vice versa*. Despite the conservation of hydrophobic residues in the characteristic heptad pattern, inverting their sequence significantly alters the architecture of the hydrophobic core.

The pair radial distribution function of the Cβ atoms of the hydrophobic residues provide an estimation of the extent of the hydrophobic core. The results for the three protein models are presented in Fig. 8. Reported values for rRop are given as the average across two independent simulation runs, whereas their comparison is provided in Fig. S12. Starting from the parent protein, wtRop, a pronounced peak at short distances is observed, indicating a tightly packed hydrophobic core. The

Table 2 Average number of the various components of hydrogen bonds for the three protein models. Hydrogen bonds for rRop models are given as the average across two independent simulation runs

Systems	⟨P–P⟩	⟨Ma–Mb⟩	⟨Ma–Ma⟩	⟨Mb–Mb⟩	⟨P–W⟩
rRop parallel	105.44 ± 1.1	6.63 ± 0.6	50.70 ± 2.08	48.13 ± 2.6	328.73 ± 3.5
rRop antiparallel	103.54 ± 1.5	9.02 ± 3.4	46.56 ± 1.5	47.01 ± 4.8	328.70 ± 1.0
wtRop	125.2 ± 1.9	7.3 ± 0.6	60.2 ± 1.2	58.6 ± 0.2	303.3 ± 2.9

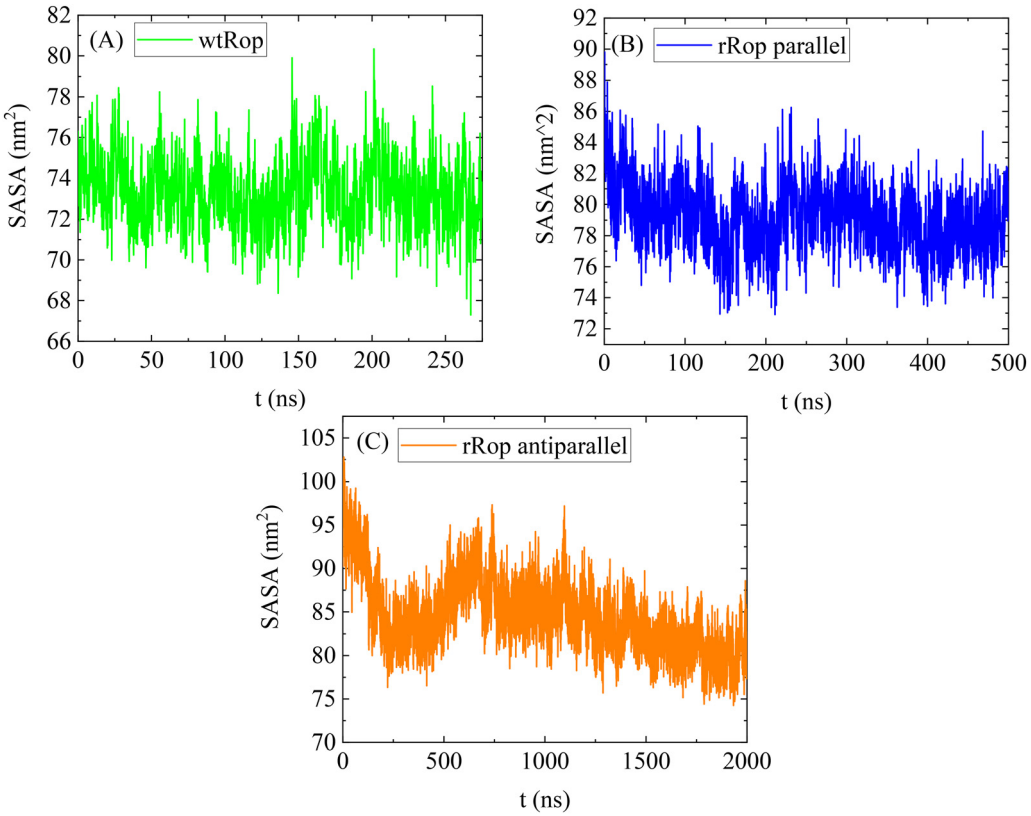


Fig. 7 Time evolution of the solvent-accessible surface area (SASA) of: (A) wtRop, (B) rRop parallel, and (C) rRop antiparallel.

parallel rRop retains the peak, but its intensity is reduced relative to wtRop. In contrast, the antiparallel protein exhibits a clear disruption of the hydrophobic core, characterized by a significantly lower peak shifted toward longer distances. This loss of hydrophobic packing aligns with findings by Zhang, Weber, and Zhou, who systematically examined native-sequence-reversed proteins and demonstrated that while sequence reversal preserves the overall hydrophobicity patterning and secondary-structure propensity, it frequently disrupts native hydrophobic core packing.[18]

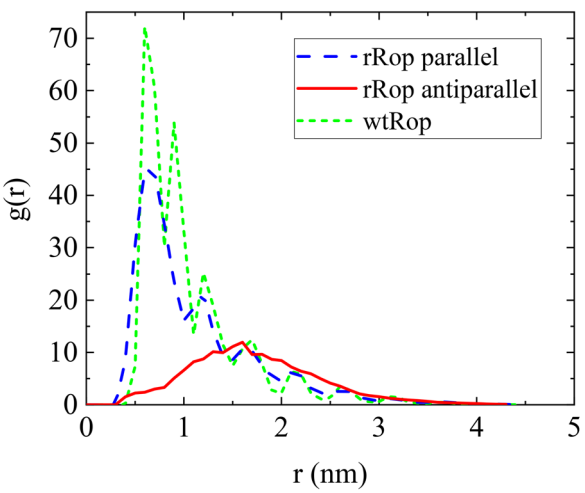


Fig. 8 Pair radial distribution function of the inter-monomer Cβ atoms of the hydrophobic residues of wtRop (green dotted line), rRop antiparallel (orange line), rRop parallel (blue dashed line). Reported values for rRop models are given as the average across two independent simulation runs.

4. WTmetaD simulations

The four collective variables employed in the WTmetaD simulations can be grouped into two categories: inter-monomer CVs, describing the relative arrangement of the two monomers (θ, the angle between the monomer axes, and r_{cm}, the distance between their centers of mass), and intra-monomer CVs, describing the internal conformational state of each monomer (H, helicity, and S, torsion angle similarity). The angle θ quantifies the relative orientation of the two monomer axis vectors, defined as the displacement from the loop-region center of mass to the top-region center of mass of each monomer (see Fig. S1 for a graphical definition); $\theta = 0^\circ$ corresponds to a parallel orientation and $\theta = 180^\circ$ to the native antiparallel orientation of wtRop.

In the following, free energy calculations were performed using (WTmetaD) simulations at 300 K. One-dimensional free energy surface (FES) results are presented in Fig. 9A comparing the energy landscape of wtRop and the rRop models as a function of the reaction coordinate θ (CV1). The global minimum for wtRop is observed at approximately 160°, corresponding to the native antiparallel orientation of the two monomers. This result aligns with previous predictions from

 This journal is © the Owner Societies 2026

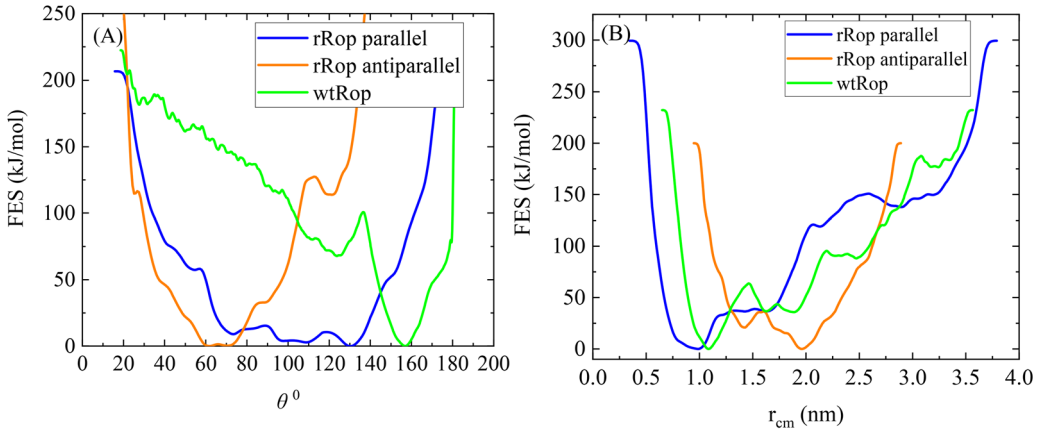


Fig. 9 One-dimensional free energy surface (FES): (A) of rRop parallel (blue line), rRop antiparallel (orange line) and wtRop (green line) as a function of the angle between monomers A and B (CV1); (B) FES of rRop parallel (blue line), rRop antiparallel (orange line) and wtRop (green line) as a function of the distance between the center of mass of monomer A and the center of mass of monomer B (CV2). Value zero is set as global minimum.

conventional MD simulations. The FES of rRop parallel reveals a broad low-energy region spanning θ values of approximately 70° to 130°. Within this basin, three shallow minima can be identified at roughly 70°, 100°, and 130°, representing distinct conformational states. The relatively low energy barriers separating these minima suggest frequent and facile transitions between them. The FES of the antiparallel rRop exhibits a dominant minimum at approximately 65°–70°, indicating that this orientation is energetically preferred. The absence of a low-energy minimum near that of the native wtRop orientation confirms a significant divergence of the reversed-sequence dimer from the geometry of the parent protein. Interestingly, the ~70° region of the rRop antiparallel model, lies within the broad, shallow basin (70°–130°) sampled by the rRop parallel model, suggesting that this orientation may represent a preferred conformational state for the reversed-sequence dimer, largely independent of the starting orientation (parallel or antiparallel monomers).

Fig. 9B shows the one-dimensional free energy profiles for rRop parallel, rRop antiparallel and wtRop as a function of the reaction coordinate r_{cm} (distance between center of mass of monomers) (CV2). For wtRop, a well-defined energy minimum is observed at approximately 1.1 nm, corresponding to the center of mass distance between monomers in the protein's native state (Fig. S3C). This deep well indicates high structural stability, although secondary local minima also appear at 1.6 nm and 1.9 nm, representing alternative, less populated configurations. The antiparallel rRop model features a global energy minimum at 1.95 nm, which diverges significantly from that of wtRop, along with a local minimum at 1.44 nm. Conversely, the parallel model's minimum occurs at 0.9 nm, slightly shorter than the one of the parent protein. These results corroborate the hydrophobic core findings (Fig. 8), where the structural similarity between wtRop and parallel rRop contrasts sharply with the core disruption observed in the antiparallel model.

Two additional collective variables were utilized for FES calculations, the helicity (CV3):

$$H = \frac{1}{2}\sum_{i}^{N}\left[1 + \cos\left(\varphi_i - \varphi_i^{\mathrm{ref}}\right)\right]$$

and the similarity of the protein backbone (CV4):

$$S = \frac{1}{2}\sum_{i}^{N}[1 + \cos(\varphi_i - \psi_i)],$$

by comparing the instantaneous dihedral angles φ and ψ. The helicity of monomer A (HA) and the helicity of monomer B (HB) are projected on x- and y- axes respectively for all three protein models in Fig. S14. The global minimum for wtRop is located at (58.08, 57.48), while the parallel and antiparallel rRop models exhibit minima at (56.51, 55.75) and (51.7, 52.49), correspondingly. These positions indicate the most stable helical conformations of monomers A and B in each system. Notably, the energy minima for the parallel rRop model align more closely with those of wtRop than the antiparallel model, suggesting a greater degree of secondary structural conservation. A similar conclusion is derived from Fig. S15 for S. For the wtRop protein, the global minimum is set at (51.51, 51.57). The global minimum for rRop antiparallel is located at (32.54, 40.83), while for rRop parallel, it is found at (47.11, 52.39). The positions of these minima represent the configurations with the highest degree of torsional similarity between monomers A and B and notably, the parallel model again more closely resembles the wtRop landscape.

Overall, the FES results indicate that neither of the two rRop models maintain the native antiparallel orientation of the parent protein, instead, the monomers appear stabilized at an intermediate angle. The antiparallel rRop model is notably less stable, exhibiting an increased inter-monomer distance compared to wtRop, whereas the parallel model largely retains its original distance. Furthermore, CV3 and CV4 reveal a greater disruption of secondary structure in the antiparallel model than in the parallel model, relative to the wild-type protein. To obtain a preliminary assessment of the correlation between the collective variables, we examined the relationship between the inter-monomer orientation angle (θ) and the center-of-mass distance (r_{cm}). Specifically, the 1D θ-biased WTmetaD simulations were reweighted using the last-bias reweighting scheme[61,62] to construct an initial 2D free energy landscape. The joint 2D free

energy landscapes for the three systems are presented in Fig. S16. For wtRop (Fig. S16C), the (r_{cm}, θ) pair corresponding to the energetic minimum, is approximately (1.3 nm, 160°). For parallel rRop (Fig. S16A), the minimum lies at approximately (0.6 nm, 130°), whereas for antiparallel rRop (Fig. S16B), the minimum is located at approximately (1.65 nm, 70°). In all three cases, quite good agreement is observed with the 1D free energy surfaces in Fig. 9A and B, confirming that selecting these individual parameters as collective variables is reasonable. However, to capture these couplings more accurately, future work could explore the correlation between pairs of collective variables, particularly the two inter-monomer CVs (θ and r_{cm}), using joint, higher-dimensional metadynamics schemes.

These observations are consistent with earlier studies on sequence-reversed helical proteins discussed in the Introduction,[22,23] which similarly reported that sequence reversal preserves the capacity to fold into compact, ordered helical structures without necessarily conserving the native fold or oligomeric arrangement. The present results extend this picture by showing that, within a single parent fold (Rop), the specific outcome of reversal depends on the resulting inter-monomer orientation itself (parallel *vs.* antiparallel), rather than being a uniform consequence of reversal alone.

5. Classical MD simulations of minimum free energy configurations

Lastly, utilizing the results of WtmetaD simulations we extracted the configurations which correspond to the global minimum energy for both rRop parallel and rRop antiparallel model and used them as initial structures for independent 100 ns classical MD simulations at 300 K. For the parallel model we used the FES of CV1 (collective variable θ), while for antiparallel we used the FES of CV2 (collective variable r_{cm}).

The initial configurations of rRop parallel and rRop antiparallel, in Fig. S18A and C, are compared with their respective final configurations in Fig. S18B and D correspondingly. On visual observation, no significant differences were found between the two corresponding configurations in either model. However, the stability of the two models is validated through the rmsd calculation, which is presented as a function of the simulation time in Fig. 10. The rmsd reported in Fig. 10 is computed relative to the initial structure of each 100 ns simulation, *i.e.*, the configurations corresponding to the global minimum of the free energies extracted from the respective CV1 (θ) and CV2 (r_{cm}) (Fig. 9). It therefore reflects the structural stability of these free-energy-minimum conformations over time. For parallel rRop, the rmsd increases slightly during the first few nanoseconds before stabilizing at ~0.35 nm. This relatively low value suggests that the protein maintains a stable structure throughout the remainder of the simulation. Conversely, the antiparallel model exhibits an abrupt increase in rmsd, reaching approximately ~0.65 nm. This significant rise suggests a marked reduction in structural stability compared to the parallel model. In addition, the rmsf values are presented in Fig. S17. In the rRop parallel model (Fig. S17A), the two monomers exhibit overall comparable rmsf values. In contrast, the rRop antiparallel model (Fig. S17B) shows a pronounced difference in the flexibility between the two monomers. Monomer B exhibits substantially higher rmsf values mainly for residues 17–49, whereas monomer A demonstrates higher rmsf values for N- and C-terminus residues. These results further validate the AlphaFold prediction, which identified the parallel configuration as the most favorable model for the reverse wtRop protein.

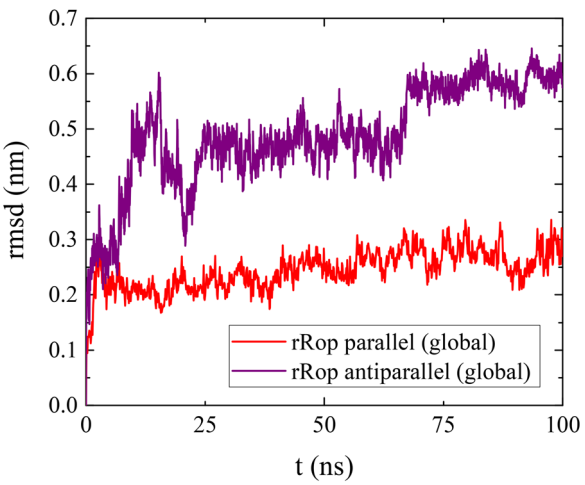


Fig. 10 Time evolution of the root mean square deviation (rmsd) of the Cα atoms of the rRop parallel (red line) and the rRop antiparallel models.

6. Conclusions

In this study, we combine classical MD simulations with well-tempered metadynamics to evaluate the stability of two reversed-sequence models of the wtRop native protein, a well-characterized coiled-coil motif. By utilizing AlphaFold, AI-driven structure predictions were first acquired for the initial structures of the unknown reverse sequence. Using enhanced sampling techniques to elucidate dynamic profiles we characterized the energetic barriers and conformational transitions within these systems. ColabFold generates five structural models for rRop: four exhibited a parallel orientation between monomers, while one adopted an antiparallel orientation similar to that of the native conformation of parent wtRop protein. Building on our previous studies of wtRop and the antiparallel rRop model, we initially focused our MD simulations on the parallel variant, subsequently comparing the results with those of the other two models of rRop.

Conformational and secondary structure analysis indicates that the parallel model possesses greater stability than its antiparallel counterpart. This is evidenced by both rmsd and rmsf metrics, including a comparatively uniform intra-monomer rmsd between the two monomers of the parallel model (Fig. S10B), in contrast to the pronounced monomer asymmetry observed in the antiparallel variant (Fig. S10A). While both reverse-sequence variants exhibit a loss of α-helicity compared to wtRop, these deviations are more pronounced in the antiparallel model. This instability is further

 This journal is © the Owner Societies 2026

reflected in the disruption of the hydrogen bond network, increased solvent accessibility (SASA), and the failure to form a robust hydrophobic core. Consequently, the parallel model retains a structural profile closer to the parent protein, compared to the antiparallel one, however, its structural integrity is also reduced.

By leveraging enhanced sampling *via* WTmetaD, we performed Free Energy Surfaces (FES) calculations for all three protein models. This approach allowed for an extensive exploration of the conformational landscape, identifying the most probable equilibrated structures located at the global or local energy minima. FES, derived from four different collective variables, demonstrated a partial similarity of the parallel rRop with the parent protein in terms of monomer center of mass distance, helicity and similarity of the protein backbone, in contrast to the antiparallel model which diverges from wtRop in all four CVs. However, both rRop models deviate from the native antiparallel orientation to stabilize at an intermediate angle. Representative structures corresponding to the FES minima for the parallel and antiparallel rRop models were subjected to additional conventional MD simulations. The resulting rmsd profiles indicated satisfactory stability for the parallel model, but highlighted instability of the antiparallel structure, corroborating the AlphaFold prediction.

The central goal of the current work is to determine the impact of sequence inversion on the core mechanisms of protein folding and overall thermodynamic stability. Building on the established classical model of the wtRop protein system, this research develops a comprehensive structural framework for engineering synthetic coiled-coil proteins.

Author contributions

Conceptualization, A.R. and V.H.; methodology, A.R. and M.A.; software, M.A.; validation, A.R., M.A. and V.H.; formal analysis, M.A.; investigation, A.R. and M.A.; resources, V.H.; data curation, M.A.; writing – original draft preparation, A.R., M.A., E.M.; writing – review & editing, A.R. and V.H.; visualization, E.M.; supervision, A.R. and V.H.; project administration, A.R.; funding acquisition, V.H. All authors have read and agreed to the published version of the manuscript.

Conflicts of interest

The authors declare no conflicts of interest.

Data availability

The PDB coordinates of all sequence-reversed coiled-coil models are provided in the supplementary information (SI). Supplementary information: Definition and Time Evolution of Collective Variables in Classical MD and WTmetaD Simulations; Fig. S1: Graphical representation of the CV angle (θ); Fig. S2: Time evolution of the unbiased MD simulation of CV1 angle (θ) of: (A) rRop parallel, (B) rRop antiparallel and (C) wtRop models; Fig. S3: Time evolution of the unbiased MD simulation of CV2 distance of: (A) rRop parallel, (B) rRop antiparallel and (C) wtRop models; Fig. S4: Time evolution of CV3 (H) from the conventional MD simulations of: (A) rRop parallel, (B) rRop antiparallel, and (C) wtRop models. Monomer A (red line) and monomer B (blue line); Fig. S5: Time evolution of CV4 (S) from the conventional MD simulations of: (A) rRop parallel, (B) rRop antiparallel, and (C) wtRop models. Monomer A (red line) and monomer B (blue line); Fig. S6: Time evolution of the collective variables during WTmetaD simulations: (A) CV1, the angle (θ) and (B) CV2, the center of mass distance between the monomers; Fig. S7: Time evolution of the collective variables during WTmetaD simulations: (A) CV3, helicity and (B) CV4, torsion similarity. Monomer A (red line) and monomer B (blue line); Results: Classical MD simulations of Parallel rRop Protein Model Fig. S8: Initial and final snapshots of (A); (B) rRop antiparallel protein; and (C); (D) wtRop protein, accordingly; Fig. S9: Time evolution of the root mean square deviation (rmsd) of the Cα atoms for (A) rRop antiparallel and (B) rRop parallel models during two independent MD simulation runs. Replica 1 and Replica 2 are shown in orange and blue, respectively; Fig. S10: Time evolution of the root mean square deviation (rmsd) of the Cα atoms of each monomer for (A) rRop antiparallel, (B) rRop parallel and (C) wtRop models. Monomer A and monomer B are shown in red and green, respectively; Fig. S11: Time evolution of the root mean square deviation (rmsd) of the Cα atoms of the rRop antiparallel; Table S1: Average number of hydrogen bonds across two independent MD simulation runs for the rRop parallel and antiparallel models; Table S2: Average SASA values, averaged over two independent MD simulation runs, for the rRop parallel and antiparallel models; Fig. S12: Pair radial distribution functions, of the inter-monomer C_β atoms of hydrophobic residues for the rRop parallel (solid lines) and rRop antiparallel (dashed lines) models across two independent MD simulations. Replica 1 and Replica 2 are shown in orange and blue, respectively; WTmetaD simulations results Fig. S13: Convergence assessment for the WTmetaD simulations for the rRop antiparallel and parallel models. (A) Time evolution of the deposited Gaussian hill heights for the rRop antiparallel model using the angle θ, as the collective variable. (B) Free-energy surfaces (FESs) reconstructed at 160, 180 and 200 ns as a function of θ for the rRop antiparallel model. (C) Time evolution of the deposited Gaussian hill heights for the rRop parallel model using the r_{cm} as the collective variable. (D) FESs reconstructed at 237, 264 and 290 ns as a function of r_{cm} for the rRop parallel model; Fig. S14: 2D free energy surface obtained from well-tempered metadynamics simulation along the helicity of monomer A (H_A) and helicity of monomer B (H_B) for (A) rRop parallel, (B) rRop antiparallel and (C) wtRop proteins. The color bar represents the free energy value in kJ mol^{-1}; Fig. S15: 2D free energy surface obtained from well-tempered metadynamics simulation along the torsion similarity of monomer A (S_A) and torsion similarity of monomer B (S_B) for (A) rRop parallel, (B) rRop antiparallel and (C) wtRop proteins. The color bar represents the free energy value in kJ mol^{-1}; Fig. S16: Reweighted 2D FES

as a function the angle between monomers A and B and the distance between the center of mass of monomer A and the center of mass of monomer B for (A) rRop parallel, (B) rRop antiparallel, and (C) wtRop. For the reweighting scheme the last bias technique was used; MD run from global minimum energy configuration Fig. S17: Root mean square fluctuations (rmsf) of Cα atoms of the: (A) rRop parallel global and (B) rRop antiparallel global models of monomer A (red line) and monomer B (blue line); Fig. S18: Graphical representation of: (A) the initial configuration (t = 0) and (B) the final configuration (t = 100 ns) of the global minimum in the rRop parallel model derived from the WtmetaD simulation using θ as the CV, (C) the initial configuration (t = 0) and (D) the final configuration (t = 100 ns) of the global minimum in the rRop antiparallel model derived from the WtmetaD simulation using rcom as the CV. See DOI: https://doi.org/10.1039/d6cp01691j.

Acknowledgements

This research received no external funding. The authors acknowledge the support of this work by computational time granted from Greek Research & Technology Network (GRNET) in the National HPC facility—ARIS for the Projects: Molecular Simulations and Free Energy Calculations of Proteins, MDMET and Simulations of Proteins *via* all atom Molecular Dynamics and Enhanced Sampling Techniques, SPMDE.

References

1 S. Tiwari, V. Atluri, A. Kaushik, A. Yndart and M. Nair, Alzheimer's disease: pathogenesis, diagnostics, and therapeutics, *Int. J. Nanomed.*, 2019, **14**, 5541–5554, DOI: 10.2147/IJN.S200490.

2 H. R. Morris, M. G. Spillantini, C. M. Sue and C. H. Williams-Gray, The pathogenesis of Parkinson's disease, *The Lancet*, 2024, **403**(10423), 293–304, DOI: 10.1016/S0140-6736(23)01478-2.

3 N. Krall, F. P. Cruz, O. Boutureira and G. J. L. Bernardes, Site-Selective Protein-Modification Chemistry for Basic Biology and Drug Development, *Nat. Chem.*, 2016, **8**(2), 103–113, DOI: 10.1038/nchem.2393.

4 L. S. Witus and M. B. Francis, Using Synthetically Modified Proteins to Make New Materials, *Acc. Chem. Res.*, 2011, **44**(9), 774–783, DOI: 10.1021/ar2001292.

5 A. Sharma, G. Gupta, T. Ahmad, S. Mansoor and B. Kaur, Enzyme Engineering: Current Trends and Future Perspectives, *Food Rev. Int.*, 2021, **37**(2), 121–154, DOI: 10.1080/87559129.2019.1695835.

6 O. Boutureira and G. J. L. Bernardes, Advances in Chemical Protein Modification, *Chem. Rev.*, 2015, **115**(5), 2174–2195, DOI: 10.1021/cr500399p.

7 D. W. Banner, M. Kokkinidis and D. Tsernoglou, *Structure of the ColEl Rop Protein at L-7 A Resolution*, 1987.

8 W. Eberle, A. Pastore, C. Sander and P. Rösch, The Structure of ColE1 Rop in Solution, *J. Biomol. NMR*, 1991, **1**(1), 71–82, DOI: 10.1007/BF01874570.

9 M. Arnittali, A. N. Rissanou, M. Amprazi, M. Kokkinidis and V. Harmandaris, Structure and Thermal Stability of wtRop and RM6 Proteins through All-Atom Molecular Dynamics Simulations and Experiments, *J. Mol. Sci.*, 2021, **22**(11), 5931, DOI: 10.3390/ijms22115931.

10 L. Castagnoli, M. Scarpa, M. Kokkinidis, D. W. Banner, D. Tsernoglou and G. Cesareni, Genetic and Structural Analysis of the ColE1 Rop (Rom) Protein, *EMBO J.*, 1989, **8**(2), 621–629, DOI: 10.1002/j.1460-2075.1989.tb03417.x.

11 M. Munson, K. S. Anderson and L. Regan, Speeding up Protein Folding: Mutations That Increase the Rate at Which Rop Folds and Unfolds by over Four Orders of Magnitude, *Fold Des.*, 1997, **2**(1), 77–87, DOI: 10.1016/S1359-0278(97)00008-4.

12 Q.-H. Ma, H.-H. Zhu and J.-Q. Han, Wheat ROP proteins modulate defense response through lignin metabolism, *Plant Sci.*, 2017, **262**, 32–38, DOI: 10.1016/j.plantsci.2017.04.017.

13 S. Yalovsky, Protein Lipid Modifications and the Regulation of ROP GTPase Function, *J. Exp. Bot.*, 2015, **66**(6), 1617–1624, DOI: 10.1093/jxb/erv057.

14 D. N. Woolfson, The Design of Coiled-Coil Structures and Assemblies, in *Advances in Protein Chemistry*, Academic Press, 2005, vol. 70, pp. 79–112, DOI: 10.1016/S0065-3233(05)70004-8.

15 N. M. Glykos, G. Cesareni and M. Kokkinidis, Protein Plasticity to the Extreme: Changing the Topology of a 4-α α-Helical Bundle with a Single Amino Acid Substitution, https://biomednet.com/elecref/0969212600700597.

16 E. Lacroix, A. R. Viguera and L. Serrano, Reading Protein Sequences Backwards, *Fold Des.*, 1998, **3**(2), 79–85, DOI: 10.1016/S1359-0278(98)00013-3.

17 M. Arnittali, A. N. Rissanou, A. Kefala, M. Kokkinidis and V. Harmandaris, Structure of Amino Acid Sequence-Reversed wtRop Protein: Insights from Atomistic Molecular Dynamics Simulations, *J. Biomol. Struct. Dyn.*, 2024, **42**(19), 9842–9856, DOI: 10.1080/07391102.2023.2252903.

18 Y. Zhang, J. K. Weber and R. Zhou, Folding and Stabilization of Native-Sequence-Reversed Proteins, *Sci. Rep.*, 2016, **6**, 25138, DOI: 10.1038/srep25138.

19 A. Kefala, M. Amprazi, E. Mylonas, D. Kotsifaki, M. Providaki, C. Pozidis, M. Fotiadou and M. Kokkinidis, Probing Protein Folding with Sequence-Reversed α-Helical Bundles, *Int. J. Mol. Sci.*, 2021, **22**(4), 1955, DOI: 10.3390/ijms22041955.

20 L. R. English, A. Tischer, A. K. Demeler, B. Demeler and S. T. Whitten, Sequence Reversal Prevents Chain Collapse and Yields Heat-Sensitive Intrinsic Disorder, *Biophys. J.*, 2018, **115**(2), 328–340, DOI: 10.1016/j.bpj.2018.06.006.

21 I. Torshin, Direct and Reversed Amino Acid Sequence Pattern Analysis: Structural Reasons for Activity of Reversed Sequence Sites and Results of Kinase Site Mutagenesis, *Biochem. J.*, 2000, **345**(3), 733–740, DOI: 10.1042/bj3450733.

22 K. A. Olszewski, A. Kolinski and J. Skolnick, Does a Backwardly Read Protein Sequence Have a Unique Native State, *Protein Eng.*, 1996, **9**(1), 5–14, DOI: 10.1093/protein/9.1.5.

23 P. R. E. Mittl, C. Deillon, D. Sargent, N. Liu, S. Klauser, R. M. Thomas, B. Gutte and M. G. Grütter, The Retro-GCN4 Leucine Zipper Sequence Forms a Stable Three-Dimensional

 This journal is © the Owner Societies 2026

Structure, *Proc. Natl. Acad. Sci. U. S. A.*, 2000, **97**(6), 2562–2566, DOI: 10.1073/pnas.97.6.2562.

24 G. H. Zerze, F. H. Stillinger and P. G. Debenedetti, Computational Investigation of Retro-Isomer Equilibrium Structures: Intrinsically Disordered, Foldable, and Cyclic Peptides, *FEBS Lett.*, 2020, **594**(1), 104–113, DOI: 10.1002/1873-3468.13558.

25 M. Amprazi, Structural Plasticity of 4-α-Helical Bundles Exemplified by the Puzzle-like Molecular Assembly of the Rop Protein, *Proc. Natl. Acad. Sci. U. S. A.*, 2014, **111**(30), 11049–11054, DOI: 10.1073/pnas.1322065111.

26 M. Munson, L. Regan, R. O'Brien and J. M. Sturtevant, Redesigning the Hydrophobic Core of a Four-Helix-Bundle Protein, *Protein Sci.*, 1994, **3**(11), 2015–2022, DOI: 10.1002/pro.5560031114.

27 Y. Levy and J. N. Onuchic, Mechanisms of Protein Assembly: Lessons from Minimalist Models, *Acc. Chem. Res.*, 2006, **39**(2), 135–142, DOI: 10.1021/ar040204a.

28 Y. Levy, S. S. Cho, T. Shen, J. N. Onuchic and P. G. Wolynes, Symmetry and Frustration in Protein Energy Landscapes: A near Degeneracy Resolves the Rop Dimer-Folding Mystery, 2004, https://www.pnas.org.

29 N. M. Glykos, Y. Papanikolau, M. Vlassi, D. Kotsifaki, G. Cesareni and M. Kokkinidis, Loopless Rop: Structure and Dynamics of an Engineered Homotetrameric Variant of the Repressor of Primer Protein, *Biochemistry*, 2006, **45**(36), 10905–10919, DOI: 10.1021/bi060833n.

30 D. Sala, F. Engelberger, H. S. Mchaourab and J. Meiler, Modeling Conformational States of Proteins with AlphaFold, 2023, DOI: 10.1016/j.sbi.2023.102645.

31 J. Jumper, Highly Accurate Protein Structure Prediction with AlphaFold, *Nature*, 2021, **596**(7873), 583–589, DOI: 10.1038/s41586-021-03819-2.

32 K. Tunyasuvunakool, Highly Accurate Protein Structure Prediction for the Human Proteome, *Nature*, 2021, **596**(7873), 590–596, DOI: 10.1038/s41586-021-03828-1.

33 J. Skolnick, M. Gao, H. Zhou and S. Singh, AlphaFold 2: Why It Works and Its Implications for Understanding the Relationships of Protein Sequence, Structure, and Function, *J. Chem. Inf. Model.*, 2021, **61**(10), 4827–4831, DOI: 10.1021/acs.jcim.1c01114.

34 A. Charpentier, D. Mignon, S. Barbe, J. Cortes, T. Schiex, T. Simonson and D. Allouche, Variable Neighborhood Search with Cost Function Networks To Solve Large Computational Protein Design Problems, *J. Chem. Inf. Model.*, 2019, **59**(1), 127–136, DOI: 10.1021/acs.jcim.8b00510.

35 P. S. F. C. Gomes, D. E. B. Gomes and R. C. Bernardi, Protein Structure Prediction in the Era of AI: Challenges and Limitations When Applying to in Silico Force Spectroscopy, *Front. Bioinform.*, 2022, **2**, 983306, DOI: 10.3389/fbinf.2022.983306.

36 P. Mahinthichaichan, R. Liu, Q. N. Vo, C. R. Ellis, L. Stavitskaya and J. Shen, Structure-Kinetics Relationships of Opioids from Metadynamics and Machine Learning Analysis, *J. Chem. Inf. Model.*, 2023, **63**(7), 2196–2206, DOI: 10.1021/acs.jcim.3c00069.

37 Z. Hu and J. Marti, Well-Tempered Metadynamics Calculations of Free Energy Surfaces of Benzothiadiazine Derivatives in Aqueous Solution, *bioRxiv*, 2023, **11**(15), 567238, DOI: 10.1101/2023.11.15.567238.

38 R. Capelli, A. J. Menke, H. Pan, B. G. Janesko, E. E. Simanek and G. M. Pavan, Well-Tempered Metadynamics Simulations Predict the Structural and Dynamic Properties of a Chiral 24-Atom Macrocycle in Solution, *ACS Omega*, 2022, **7**(34), 30291–30296, DOI: 10.1021/acsomega.2c03536.

39 B. Oruganti and R. Friedman, Activation of Abl1 Kinase Explored Using Well-Tempered Metadynamics Simulations on an Essential Dynamics Sampled Path, *J. Chem. Theory Comput.*, 2021, **17**(11), 7260–7270, DOI: 10.1021/acs.jctc.1c00505.

40 M. Han, J. Xu, Y. Ren and J. Li, Simulation of Coupled Folding and Binding of an Intrinsically Disordered Protein in Explicit Solvent with Metadynamics, *J. Mol. Graph. Model.*, 2016, **68**, 114–127, DOI: 10.1016/j.jmgm.2016.06.015.

41 F. E. S. Mosa, S. AlRawashdeh, A. O. S. El-Kadi and K. Barakat, Investigating the Aryl Hydrocarbon Receptor Agonist/Antagonist Conformational Switch Using Well-Tempered Metadynamics Simulations, *J. Chem. Inf. Model.*, 2024, **64**(6), 2021–2034, DOI: 10.1021/acs.jcim.4c00169.

42 J. Das, Microscopic Insights into a Ligand Escape Pathway and Energetics in Leucine–Isoleucine–Valine Binding Protein, *ACS Omega*, 2026, **11**(15), 22787–22795, DOI: 10.1021/acsomega.5c12025.

43 H. Nadwa, Z. Brotzakis, A. Santucci, D. Braconi and M. Vendruscolo, Destabilization of Helix III Initiates Early Serum Amyloid A Misfolding by Exposing Its Amyloidogenic Core, *J. Phys. Chem. Lett.*, 2025, **16**, 13190–13198, DOI: 10.1021/acs.jpclett.5c03467.

44 Z. F. Brotzakis, T. Löhr, S. Truong, S. Hoff, M. Bonomi and M. Vendruscolo, Determination of the Structure and Dynamics of the Fuzzy Coat of an Amyloid Fibril of IAPP Using Cryo-Electron Microscopy, *Biochemistry*, 2023, **62**, 2407–2416.

45 X. Gong, Well-Tempered Metadynamics Simulations Combined with Free Energy Landscape Analysis Uncover the Conformational Transition Pathway of the DYG Motif in LRRK2, *ACS Chem. Neurosci.*, 2025, **16**(15), 2800–2811, DOI: 10.1021/acschemneuro.5c00054.

46 H. Zhang, E. J. K. Lim and L. Lu, Investigating the Stability of Dengue Virus Envelope Protein Dimer Using Well-Tempered Metadynamics Simulations, *Proteins: Struct., Funct., Bioinf.*, 2020, **88**(5), 643–653, DOI: 10.1002/prot.25844.

47 R. Zhou and M. Duan, Metadynamics Simulations to Study the Structural Ensembles and Binding Processes of Intrinsically Disordered Proteins, in *Computational Peptide Science: Methods and Protocols*, ed. T. Simonson, Springer US, New York, NY, 2022, pp. 169–178, DOI: 10.1007/978-1-0716-1855-4_9.

48 X. Zhou, M. Shi, X. Wang and D. Xu, Exploring the Binding Mechanism of a Supramolecular Tweezer CLR01 to 14-3-3σ Protein via Well-Tempered Metadynamics, *Front. Chem.*, 2022, **10**, 921695, DOI: 10.3389/fchem.2022.921695.

49 K. Zuo, A. Kranjc, R. Capelli, G. Rossetti, R. Nechushtai and P. Carloni, Metadynamics Simulations of Ligands Binding to Protein Surfaces: A Novel Tool for Rational Drug Design,

Phys. Chem. Chem. Phys., 2023, **25**(20), 13819–13824, DOI: 10.1039/d3cp01388j.
50 F. Fratev, PPARγ Helix 12 Exhibits an Antagonist Conformation, *Phys. Chem. Chem. Phys.*, 2016, **18**(13), 9272–9280, DOI: 10.1039/C5CP06729D.
51 W. L. Delano The PyMOL Molecular Graphics System; 2002.
52 M. J. Abraham, T. Murtola, R. Schulz, S. Páll, J. C. Smith, B. Hess and E. Lindahl, GROMACS: High Performance Molecular Simulations through Multi-Level Parallelism from Laptops to Supercomputers, *SoftwareX*, 2015, **1–2**, 19–25, DOI: 10.1016/j.softx.2015.06.001.
53 C. Oostenbrink, A. Villa, A. E. Mark and W. F. Van Gunsteren, A Biomolecular Force Field Based on the Free Enthalpy of Hydration and Solvation: The GROMOS Force-Field Parameter Sets 53A5 and 53A6, *J. Comput. Chem.*, 2004, **25**(13), 1656–1676, DOI: 10.1002/jcc.20090.
54 H. J. C. Berendsen, J. R. Grigera and T. P. Straatsma, The Missing Term in Effective Pair Potentials, *J. Phys. Chem.*, 1987, **91**(24), 6269–6271, DOI: 10.1021/j100308a038.
55 G. Bussi, D. Donadio and M. Parrinello, Canonical Sampling through Velocity Rescaling, *J. Chem. Phys.*, 2007, **126**(1), 014101, DOI: 10.1063/1.2408420.
56 H. J. C. Berendsen, J. P. M. Postma, W. F. van Gunsteren, A. DiNola and J. R. Haak, Molecular Dynamics with Coupling to an External Bath, *J. Chem. Phys.*, 1984, **81**(8), 3684–3690, DOI: 10.1063/1.448118.
57 V. Spiwok, M. Kurečka and A. Křenek, Collective Variable for Metadynamics Derived From AlphaFold Output, *Front. Mol. Biosci.*, 2022, **9**, 878133, DOI: 10.3389/fmolb.2022.878133.
58 A. Barducci, M. Bonomi and M. Parrinello, Metadynamics, *WIREs Comput. Mol. Sci.*, 2011, **1**(5), 826–843, DOI: 10.1002/wcms.31.
59 P. G. Bolhuis, Sampling Kinetic Protein Folding Pathways Using All-Atom Models, in *Computer Simulations in Condensed Matter Systems: From Materials to Chemical Biology*, ed. M. Ferrario, G. Ciccotti, K. Binder, Springer Berlin Heidelberg, Berlin, Heidelberg, 2006, vol. 1, pp. 393–433, DOI: 10.1007/3-540-35273-2_11.
60 W. Kabsch and C. Sander, Dictionary of Protein Secondary Structure: Pattern Recognition of Hydrogen-Bonded and Geometrical Features, *Biopolymers*, 1983, **22**(12), 2577–2637, DOI: 10.1002/bip.360221211.
61 G. Bussi and A. Laio, Using Metadynamics to Explore Complex Free-Energy Landscapes, *Nat. Rev. Phys.*, 2020, **2**(4), 200–212, DOI: 10.1038/s42254-020-0153-0.
62 D. Branduardi, G. Bussi and M. Parrinello, Metadynamics with Adaptive Gaussians, *J. Chem. Theory Comput.*, 2012, **8**(7), 2247–2254, DOI: 10.1021/ct3002464.

 This journal is © the Owner Societies 2026